AIAA SciTech Forum
12-16 January 2026, Orlando, FL
AIAA SCITECH 2026 Forum

10.2514/6.2026-2461

Machine Learning-Guided Design of Binary Ionic Liquid Mixtures for Spacecraft Thermal Control

Elif Acar*, Prithwish Biswas†, and Sadaf Sobhani‡
Cornell University, Ithaca, New York, 14853, USA

This study investigates the use of binary ionic liquid (IL) mixtures as advanced heat transfer fluids, with the aim of identifying combinations that exhibit improved thermophysical properties compared to their pure IL components. The focus is on predicting viscosity using machine learning (ML) models enhanced with physics-based descriptors. Thermophysical property data were collected for 698 binary mixtures, alongside extensive pure IL datasets used for reference. Multiple feature-generation strategies were explored to represent binary systems, including ideal mixing rules for conventional molecular descriptors to capture composition-dependent interactions, as well as quantum chemical surface charge densities and chemical potentials to incorporate structure-dependent realistic interactions. Initial analysis shows non-ideal behavior in viscosity with respect to both temperature and mole fraction, supporting the potential of binary systems to offer more favorable properties. Deep neural networks were developed for pure ILs and mixtures, and feature reduction techniques were applied to identify the most informative structural and energetic descriptors. This work provides a foundational step toward a generalizable ML framework for predicting binary IL behavior and supports future data-driven design of IL mixtures for single-phase thermal control loops, particularly for aerospace applications in extreme environments.

I. Introduction

Spacecraft operating beyond low Earth orbit, such as those destined for the Moon, Mars, or deep space, face thermal conditions that exceed the capabilities of passive thermal control systems alone. In these missions, active thermal control systems, most commonly single-phase pumped fluid loops in single- or two-fluid configurations, are critical for maintaining components within operational temperature limits. In a typical loop, a mechanical pump circulates the fluid through a closed network of tubing and heat exchangers, where it absorbs heat from components and rejects it to space through a radiator. Such systems have been implemented on both robotic (e.g., Mars Pathfinder, Mars Exploration Rovers, and Mars 2020) and human spacecraft missions (e.g., Apollo, Gemini, Space Shuttle, and Orion) [1–5]. Regardless of whether the fluid is used in a single- or two-fluid architecture, its performance is governed by its viscosity, freeze tolerance, heat capacity, and stability.

A variety of fluids have been used in single-phase pumped fluid loops, including water, glycol, ammonia, and engineered liquids such as Freon-21, HFE-7200, and Fluorinert FC-72 [5]. While these fluids have proven to be effective in past missions, many present drawbacks such as high freezing points limit their applicability. Moreover, many fluorinated working fluids have been discontinued due to regulatory restrictions related to perfluoroalkyl (PFAS) emissions [6–10]. As missions are increasingly targeting more extreme thermal environments, the demand for advanced working fluids with improved thermophysical performance has grown. Fluids with low freezing points or those that exhibit deep supercooling and remain liquid under extreme cold are essential to avoid system freeze-up. Additionally, low-viscosity is desirable to reduce pressure drops in the loop, decreasing the mechanical pump power required and ultimately lowering system mass and energy consumption [2]. In addition, enhancing specific heat increases the amount of thermal energy carried per unit mass, and higher thermal conductivity improves conjugate heat transfer, further improving overall system efficiency [11]. To surpass the limitations of traditional working fluids, new liquids with tailored thermophysical properties must be designed to meet the demands of extreme space environments and advanced system-level constraints.

Ionic liquids (ILs) are proposed as a frontier class of working fluids due to their modular chemical structure, enabling extensive tunability through independent selection of cations and anions [12]. Additionally, ILs' inherent high thermal

*PhD Student, Sibley School of Mechanical and Aerospace Engineering, AIAA Student Member.
†Postdoctoral Associate, Sibley School of Mechanical and Aerospace Engineering.
‡Assistant Professor, Sibley School of Mechanical and Aerospace Engineering, AIAA Member.

stability and low vapor pressure make them well-suited for operation in demanding space environments [13, 14]. Even though the vast chemical design space of ILs, estimated to be over 10^8 cation-anion combinations, offers exciting opportunities, it also presents a significant challenge for conventional screening methods. Machine learning (ML) has emerged as a powerful tool to efficiently predict key thermophysical properties and identify promising candidates. Previous work has focused on predicting pure ILs with low viscosity and liquid phase transition temperature [12].

While such advances provide a foundation for pure-component screening, far less attention has been given to IL mixtures. Binary IL mixtures introduce an additional degree of tunability by enabling composition-based adjustment of properties on top of structural design. The viscosity–composition relationship of IL mixtures remains understudied compared to mixing effects in conventional molten-salt systems [15–17]. Moreover, classical concepts such as melting-point depression in small-molecule mixtures do not translate directly to ILs: large, asymmetric ions tend to form glasses instead of ordered crystals, leading to extended supercooling and rendering melting-point-based mixture heuristics less meaningful. Consequently, viscosity emerges as a more practically important and physically informative property for IL mixture design.

Developing ML models for IL mixtures requires mixture representations capable of capturing non-ideal composition-dependent interactions. Methods used in prior studies include mole-fraction-weighted molecular descriptors, explicit inclusion of mole fraction as a feature, group-contribution approaches, and physics-based representations derived from COSMO-RS σ-profile [18–24]. Group-contribution models offer interpretability but cannot generalize to ILs containing motifs absent from the training data. Conductor-like Screening Model for Real Solvents (COSMO-RS) enables computation of surface charge density distributions typically known as sigma profiles (σ-profiles) and thermodynamic properties such as chemical potentials, yet σ-profile-based features have seen limited use for viscosity prediction, and the integration of COSMO-RS thermodynamic descriptors into ML models remains largely unexplored.

These gaps highlight the need for mixture property–prediction frameworks that combine chemical structure, mixture physics, and ML-based nonlinear modeling. As IL discovery efforts increasingly adopt iterative workflows—where computational screening guides synthesis, experimental data feed model retraining, and property predictions inform system-level evaluation—predictive models for binary mixtures represent a critical enabling capability for expanding beyond pure-component design.

The objective of this study is to develop a generalizable, physics-guided ML framework for predicting viscosity of binary IL mixtures. We compare multiple mixture-representation strategies, evaluate their performance across different dataset-splitting schemes, and analyze nonlinear composition effects of features. The results provide fundamental insights into IL mixing behavior and establish a foundation for data-driven mixture design in advanced spacecraft thermal-control applications.

II. Methodology

A. Dataset gathering and preparation

Thermophysical property data for IL binary mixtures were collected from the NIST ILThermo Database (SRD#147) v2.0 [14, 25]. The database includes several important properties measured at atmospheric pressure, such as eutectic and monotectic temperatures, viscosity, density, heat capacity, and thermal conductivity. For viscosity, the dataset contains 698 unique binary mixtures formed from 512 different ILs and molecular solvents.

Figure 1 shows how pure ILs and binary mixtures are distributed across temperature for viscosity. Compared to pure ILs, the amount of available mixture data is much smaller and concentrated in narrower temperature ranges. Pure ILs span a wider temperature window and display smoother overall trends, yet both pure ILs and mixtures exhibit strong nonlinear behavior in viscosity as temperature changes. This nonlinearity is especially pronounced in the mixture data, where composition also contributes to additional curvature and variation. Even with the limited and uneven sampling of mixtures, many systems show promising characteristics. Several binary mixtures reach lower viscosities at low temperatures and extend into viscosity ranges not observed for their individual pure components. These observations suggest that mixing can produce favorable viscosity behavior and highlight the value of developing reliable predictive models for binary IL mixtures.

Not all available mixtures could be used in this study. Some mixtures were excluded because chemical potential descriptors were not yet generated for them, and all feature combinations needed to be tested on the same dataset for fair comparison. After filtering, the mixture dataset used for model development included 88 unique IL pairs, 407 unique mixture compositions (defined by IL1, IL2, and mole fraction), and a total of 3,637 temperature-dependent data points.

A similar filtering step was applied to the pure IL dataset, since some of the newly added descriptors could not be

computed for every compound. To ensure that all feature combinations were evaluated on the same set of ILs, entries with missing descriptor values were removed. After this filtering, the final pure IL dataset contained 963 unique ILs and approximately 11,500 temperature-dependent data points.

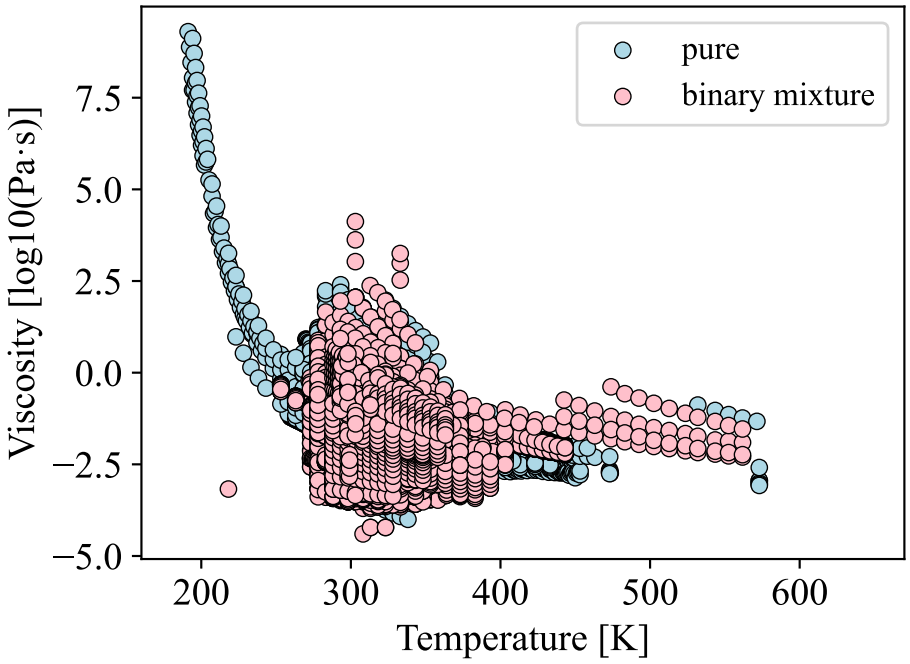

Fig. 1 Viscosity distribution as a function of temperature of IL binary mixtures and pure ILs in liquid phase at atmospheric pressure (scaled to log10 due to their wide data range).

B. Featurization

Featurization refers to translating the physical and chemical identity of ILs into numerical inputs that ML models can interpret. The goal of this step is to encode structural, energetic, and compositional information in a way that allows models to learn meaningful structure–property relationships. In this work, three types of descriptors are considered: molecular descriptors, surface charge density (σ-profiles), and chemical potential features. These feature families are evaluated individually and in combination to determine which representations are most suitable for predicting the thermophysical properties of both pure ILs and binary mixtures.

1. Molecular descriptors

Molecular descriptors were generated using SMILES representations of each cation and anion. Using RDKit, 210 descriptors were computed for every ion pair [26, 27]. This approach has been successfully applied in prior pure-IL studies and provides a broad structural representation including topology, partial charge distributions, steric features, and connectivity indices [12, 28–33]. Composition in the NIST ILThermo dataset appears in several formats (i.e., mole fraction, weight fraction, molality, molarity, mole ratio, mass ratio, volume fraction, and moles per mass of solution). Thus, all composition types were converted to mole fraction for consistency. To embed mole-fraction effects into molecular descriptors, several combination strategies were implemented. These strategies reflect different assumptions about how descriptors from IL_1 and IL_2 combine to influence the resulting mixture. The following composition-dependent molecular descriptor combination strategies were evaluated [18]:

- Mole-fraction-weighted average:

$$D = x\, d_1 + (1 - x)\, d_2 \tag{1}$$

- Weighted difference:

$$D = |\, x\, d_1 - (1 - x)\, d_2 \,| \tag{2}$$

- Square mole fraction contributions:

$$D = x^2 d_1 + (1-x)^2 d_2 \tag{3}$$

- Square molar contribution:

$$D = (x\, d_1 + (1-x)\, d_2)^2 \tag{4}$$

Each binary mixture was initially represented by approximately 420 molecular descriptors from IL_1 and 420 from IL_2. These descriptors were first combined using the selected composition-dependent mixing rules (Eqs. 1–4). After applying the mixing rules, the individual IL_1 and IL_2 descriptors were discarded, and only the mixture-derived descriptors were retained. This procedure resulted in a set of 210 combined descriptors for each mixture, each carrying the contribution of mole fraction. Feature reduction was then applied to these 210 descriptors by removing those with zero variance, NaN values, or one of the fully correlated pairs, followed by a LASSO-based selection to eliminate descriptors with low predictive relevance. Because each mixing rule produces a different feature representation and therefore a different relationship with the target property, LASSO selects a unique subset of features for each case [34, 35]. The resulting reduced sets are case-specific but consistently compact and informative for modeling mixture properties.

2. Surface charge density (σ-profiles)

To incorporate physically meaningful representations of intermolecular interactions into the feature space, we employed COSMO-RS (Conductor-like Screening Model for Real Solvents) to compute σ-profiles for each ion [36, 37]. COSMO-RS provides a computationally inexpensive framework for evaluating equilibrium energetics of molecular liquids. To compute thermodynamic properties such as the chemical potential, each molecule is represented by a surface screening charge density distribution, commonly referred to as the σ-profile. The σ-profile is obtained through two Density Functional Theory (DFT) based steps. First, gas-phase geometry optimizations were performed for the isolated cations and anions in order to obtain their ground-state minimum-energy structures. The optimizations employed the PBE (Perdew–Burke–Ernzerhof) exchange–correlation functional with a triple-ζ polarized (TZP) Slater-type orbital basis and a small frozen core. Atomic coordinates were iteratively updated along the negative gradient of the total electronic energy until the change in total energy per atom between successive steps was below 10^{-5} Hartree per atom. The resulting structures were then accepted as local minima. Second, single-point COSMO calculations were carried out on the optimized geometries under perfect-conductor boundary conditions to obtain the σ-profiles. A molecular cavity was constructed by superimposing the van der Waals spheres of all atoms in the molecule, after which the cavity surface was discretized into small surface segments. The screening (image) charge density on each segment was computed such that the electrostatic potential inside the cavity remained constant. The resulting probability distribution $p(\sigma)$ of the image charge densities defines the σ-profile for the molecule.

The σ-profile of individual cations ($p(\sigma)_{cation}$) and anions ($p(\sigma)_{anion}$) were computed by the above methodology. A mole fraction weighted average of the σ-profile of $p(\sigma)_{cation}$ and anions $p(\sigma)_{anion}$ represent the σ-profile of the IL. Hence, for ILs consisting of monovalent ions the σ-profile of the IL ($p(\sigma)_{IL}$) is given by:

$$p(\sigma)_{\mathrm{IL}} = 0.5p(\sigma)_{cation} + 0.5p(\sigma)_{anion} \tag{5}$$

Similarly for binary mixtures of ILs the σ-profiles of individual ILs, $p(\sigma)_{IL_1}$ and $p(\sigma)_{IL_2}$, were calculated using Eq. (5) and then the σ-profile of the whole mixture ($p(\sigma)_{mix}$)was calculated using Eq. (6):

$$p(\sigma)_{\mathrm{mix}} = xp(\sigma)_{IL_1} + (1-x)p(\sigma)_{IL_2} \tag{6}$$

where x is the mole fraction of the first IL. For ML modeling, the σ-profiles, $p(\sigma)_{IL}$ for pure ILs or $p(\sigma)_{mix}$) for mixtures, were segregated into six region-integrated features corresponding to chemically meaningful domains (hydrogen-bond donor, acceptor, non-polar, etc.) and the area of each region ($\int \mathrm{p}(\sigma)\mathrm{d}\sigma$) were used as descriptors. Figure 2 compares σ-profiles with viscosity behavior for four example ILs. Although σ-profiles provide a compact and physically interpretable description of intermolecular interactions, strong interactions generally lead to higher viscosity. However, this trend is not universal as viscosity is a dynamic property affected by other aspects such as molecular packing and flexibility. For instance, the red and pink ILs show highly similar σ-profiles but differ in viscosity by several orders of magnitude. On the other hand, the green IL has a distinct σ-profile with the highest peak, yet its viscosity trend is closer to that of the blue IL. Additionally, the σ-profiles represent the ground state surface charge densities. The intermolecular interactions at a finite temperature will be governed by thermodynamics, which necessitates the computation of the free energy or the chemical potential of the systems.

3. Chemical potential

To capture energetic interactions that σ-profiles alone cannot describe, chemical potential distributions of the surface segments were obtained by the following equation in a self-consistent manner:

$$\mu(\sigma) = k_B T \ln \int p(\sigma) \exp\left[-\frac{E_{\text{int}}(\sigma, \sigma') - \mu(\sigma')}{k_B T}\right] d\sigma', \tag{7}$$

where E_{int} is the sum of the hydrogen-bonding energy and the misfit energy [38]. The misfit energy represents the energetic cost of removing an exposed surface segment when two ions come into contact. Cations and anions interact through different surface segments, and once they form the liquid phase, the contacting segments are no longer part of the external surface but become internal to the ion pair or cluster. The misfit energy is zero when the charges on the interacting segments cancel exactly, as in simple salts such as NaCl. In ILs, the ions are large and their charges are delocalized. At finite temperature, equilibrium self-diffusion causes different cation segments to contact different anion segments over time. Exact cancellation of the charges is therefore unlikely, which leads to a finite misfit energy in ILs.

The chemical potential profile of a pure IL ($\mu(\sigma)_{IL}$) or a binary IL mixture ($\mu(\sigma)_{mix}$) can be represented as a mole-fraction-weighted average of the corresponding profiles of the constituent ions similar to the σ-profiles as described in Eqs. (5 and 6).

The chemical potential of adding an arbitrary ion or molecule X, with a σ-profile $p_X(\sigma)$, to a liquid Y, with a chemical potential profile $\mu_Y(\sigma)$, is given by

$$\mu_X = \int p_X(\sigma)\, \mu_Y(\sigma)\, d\sigma. \tag{8}$$

Hence, using Eq. (8) the chemical potentials of inserting individual cation and anion were first computed using Eqs. (9) and (10). Then the chemical potential (μ_{pureIL})of inserting the whole IL molecules (cation + anion) to themselves were calculated as a weighted average of the chemical potential of adding individual cation and anions as represented by Eq.(11).

$$\mu_{cation} = \int p_{cation}(\sigma)\, \mu_{IL}(\sigma)\, d\sigma \tag{9}$$

$$\mu_{anion} = \int p_{anion}(\sigma)\, \mu_{IL}(\sigma)\, d\sigma \tag{10}$$

$$\mu_{\text{pureIL}} = 0.5\mu_{cation} + 0.5\mu_{anion} \tag{11}$$

Similarly for the binary mixtures the chemical potential profile of individual ionic ILs were first computed using Eq. (7). Then the chemical potential profile of the whole binary mixture ($\mu(\sigma)_{binaryIL}$) is represented as the mole fraction weighted average of the chemical potential profile of the individual components as represented by Eq. (12).

$$\mu(\sigma)_{\text{binaryIL}} = x\mu(\sigma)_{IL_1} + (1-x)\mu(\sigma)_{IL_2} \tag{12}$$

Then $\mu(\sigma)_{binaryIL}$ calculated from Eq. (12) was used to compute the chemical potential of inserting each of the 4 constituent ions of IL_1 and IL_2 using Eq. (13).

$$\mu_{cation/anion} = \int p_{cation/anion}(\sigma)\, \mu_{binaryIL}(\sigma)\, d\sigma \tag{13}$$

The chemical potential of the whole binary mixture was represented as the mole fraction weighted average of adding all the four ions to the binary mixture as represented by Eq. (14).

$$\mu_{\text{mix}} = x(\mu_{cation_{IL1}} + \mu_{anion_{IL1}}) + (1-x)(\mu_{cation_{IL2}} + \mu_{anion_{IL2}}) \tag{14}$$

The computed average μ_{pureIL} and μ_{mix} were used as descriptors for training the ML models for pure ILs and binary mixture of ILs respectively.

4. Feature reduction

For pure ILs, seven different feature combinations were tested, including each descriptor family on its own (molecular descriptors, σ-profiles, and chemical potential) as well as all pairwise and full three-way combinations. The final number of features after reduction for each case is listed in Table 1. LASSO-based feature selection was applied only to the molecular-descriptor-containing feature sets, since these initially contained a high number of variables. In contrast, the σ-profile and chemical potential feature sets already had very few features, so LASSO was therefore not applied to those cases.

For binary mixtures, the same seven combinations were constructed using the mixture-specific descriptors. The final reduced feature counts for each mixture feature set are shown in Table 2. These tables summarize the feature space used for model training and allow direct comparison of the different descriptor families.

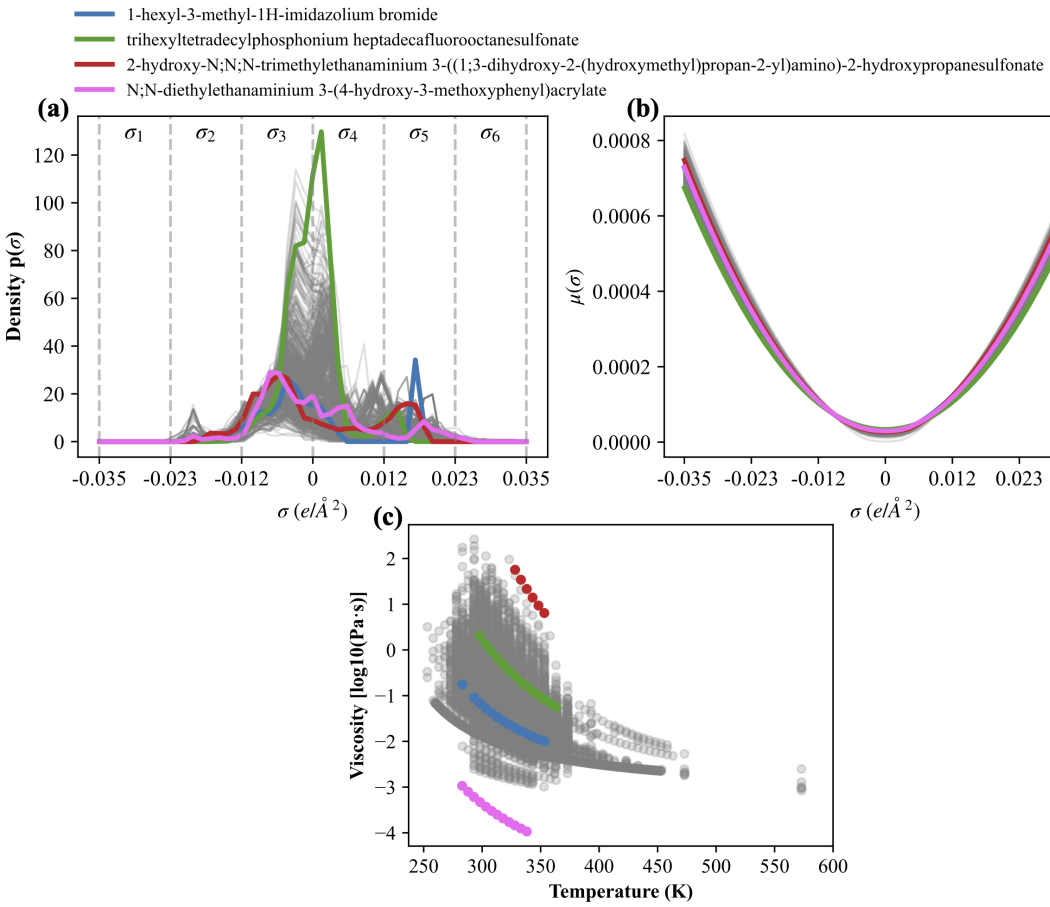

Fig. 2 Comparison of σ-profile distributions and viscosity behavior of selected pure ILs. (a) σ-profiles for several representative ILs, highlighting regions associated with hydrogen-bond donor and acceptor tendencies. (b) Corresponding viscosity trends as a function of temperature for the same ILs, illustrating that similar σ-profiles can lead to different viscosity behaviors.

Table 1 Feature combinations evaluated for pure ILs and the number of features after reduction (temperature included in all cases).

Case	Feature Set	Reduced Feature Count
MD	Molecular descriptors	82
Sigma	σ-profiles integrals	7
Chempot	Chemical potential descriptors (μ_{sum})	2
MD + Sigma	Combined molecular and sigma features	96
Sigma + Chempot	Combined sigma and chemical potential features	8
MD + Chempot	Combined molecular and chemical potential features	74
MD + Sigma + Chempot	Full combined feature set	62

Table 2 Binary mixture feature combinations and reduced feature counts, temperature included as a feature (for 50% mole frac | all mixture data).

Case	Binary Mixture Feature Set	Reduced Features
MD	• Mole-fraction-weighted average (mol_frac_avg)	19 | 15
	• Weighted difference (weighted_diff)	23 | 28
	• Square mole fraction (square_mf)	19 | 11
	• Square molar contribution (squared_contrib)	25 | 11
Sigma	σ-profiles integrals	6
Chempot	Chemical potential descriptor	2
MD + Sigma	Combined molecular (best) and sigma	25 | 10
MD + Chempot	Combined molecular (best) and chemical potential	25 | 39
Sigma + Chempot	Combined σ and chemical potential	7
MD + Sigma + Chempot	Combined molecular (best), σ, and chemical potential	25 | 12

C. Training and test dataset splitting and scaling

The pure IL dataset was divided into training (80%) and test (20%) sets by grouping unique ILs, ensuring that no IL appearing in the test set was present in the training set. This approach allows the model to be evaluated on entirely unseen ILs.

For binary mixtures, two splitting strategies were used, as illustrated in Fig. 3. In both strategies, the data were divided into training (90%) and test (10%) sets.

1) Fixed 50 mol% case: All mixtures were filtered to the closest available composition to 50 mol%. The splitting was then performed by grouping unique mixtures. This setup tests the model's ability to predict fully new binary mixtures at a single, common composition.
2) Full-composition-range case: In this case, mixtures were grouped by both identity and mole fraction before splitting. This approach evaluates how well a model can predict new compositions of mixtures that it has already partially seen.

Figure 3 shows the mapping of available mixture compositions and the resulting train/test selections for both splitting strategies. Panels (a) and (b) illustrate the distribution of mixture compositions across all binary systems, while panels (c) and (d) present the corresponding temperature–viscosity plots for the selected train and test sets in each case.

All features were scaled using Min–Max normalization to the range $[0, 1]$ to support stable model training. Viscosity values were transformed using a base-10 logarithm to reduce skewness and improve learning of temperature-dependent trends.

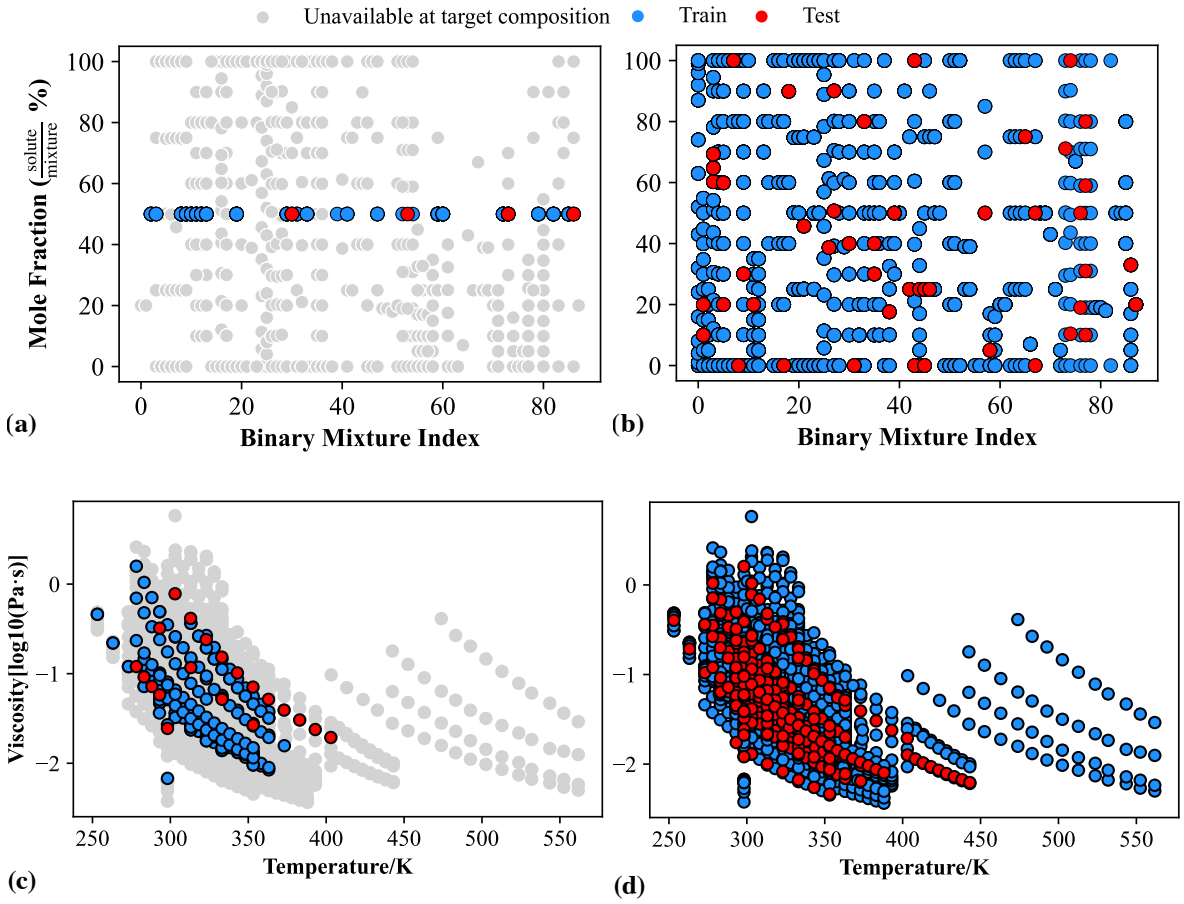

Fig. 3 Train/test splitting of binary mixtures for (a) 50 mol% and (b) all compositions. (c) and (d) show the train/test temperature–viscosity plots for each case.

D. Machine learning model development

For both pure ILs and binary mixtures, deep neural network (DNN) models were developed following the same framework used in the Acar et al [12]. A DNN was chosen because viscosity shows strong nonlinearity and complex temperature-dependent trends, and earlier results demonstrated that this architecture performed best for viscosity prediction. The overall model structure is illustrated in Fig. 4.

The model consisted of four hidden layers with 256 nodes in each layer. The ReLU activation function was used for all hidden layers, and the Adam optimizer was employed for weight updates [39]. The mean squared error (MSE) was selected as the loss function. Training was carried out for 200 epochs with a batch size of 32. Detailed descriptions of this architecture and how it was picked can be found in Acar et al., since the same model setup is used here [12]. After training, the models were evaluated using the coefficient of determination (R^2) on both the training and test datasets to assess predictive performance.

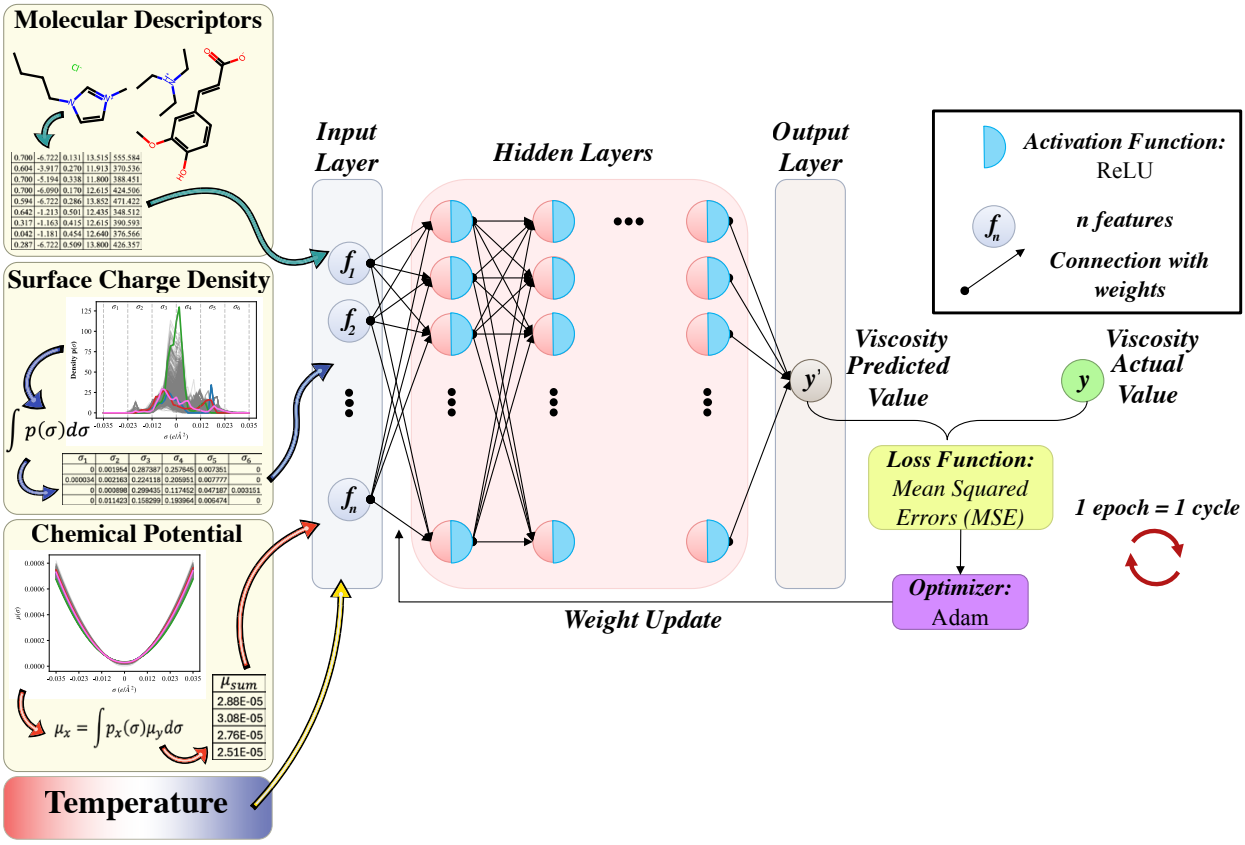

Fig. 4 Deep neural network architecture used for viscosity prediction.

III. Results and Discussion

A. Baseline Pure IL Performance

Pure IL viscosity models were first developed and evaluated to establish a baseline and to confirm that the new features behave consistently before applying them to binary mixtures. As shown in Fig. 5, models using only molecular descriptors produced strong predictive performance. This agreement validates the data preparation pipeline and confirms that the DNN architecture is suitable for capturing the highly nonlinear temperature dependence of viscosity.

When the physics-based descriptors were evaluated individually, the σ-profile features performed better than the chemical potential features, reflecting the richer polarity information encoded across the six sigma regions. Low performance on chemical potential was expected as the feature set contains only two descriptors, limiting its expressiveness. However, both feature families were able to predict viscosity with reasonable accuracy on their own, which indicates that each captures meaningful aspects of IL structure. Performance improved further when descriptors were combined. The MD + Chempot model produced the highest test accuracy, followed closely by MD + Sigma and Sigma + Chempot. The full combination of all three feature types also performed well, but did not exceed the MD + Chempot case. This suggests that, for pure ILs, the molecular descriptors benefit most from additional energetic information encoded in the chemical potential, while adding sigma information on top of both does not provide further gain. One likely explanation is that viscosity in pure ILs is influenced more strongly by local energetic interactions than by the broader polarity distribution represented by the sigma regions.

Figure 6 helps identify outliers in the behavior of the models that perform the best and provides further insight through the Shapley Additive Explanations (SHAP) analysis, which quantify the contribution of each feature to predictions [40]. In all three cases, the models show a slight tendency to overpredict viscosity. Across all feature sets, temperature remains the dominant predictor, which is consistent with the strong exponential dependence of viscosity on temperature. In the MD + Chempot model, the chemical potential descriptor μ_{sum} appears among the most influential features, together with partial-charge and volume-related descriptors, highlighting the role of local energetic environments. In the MD

+ Sigma model, at least one sigma-region integral consistently ranks among the top features, indicating that specific surface-charge-density regions influence viscosity behavior. In the σ-only model, all six sigma integrals contribute meaningfully, with the σ_5 and σ_3 regions having the strongest impact, which correspond to the hydrogen-bond donor (presence of electronegative atoms) and the near-zero polarity regions.

Overall, the pure IL results demonstrate that molecular descriptors provide a strong baseline, while physics-based descriptors introduce additional physically meaningful information. The performance trends and SHAP rankings confirm that the three descriptor families behave consistently and complement each other in intuitive ways. These observations give confidence that the same descriptor sets can be extended to binary mixtures, where composition-dependent interactions are expected to play a more significant role.

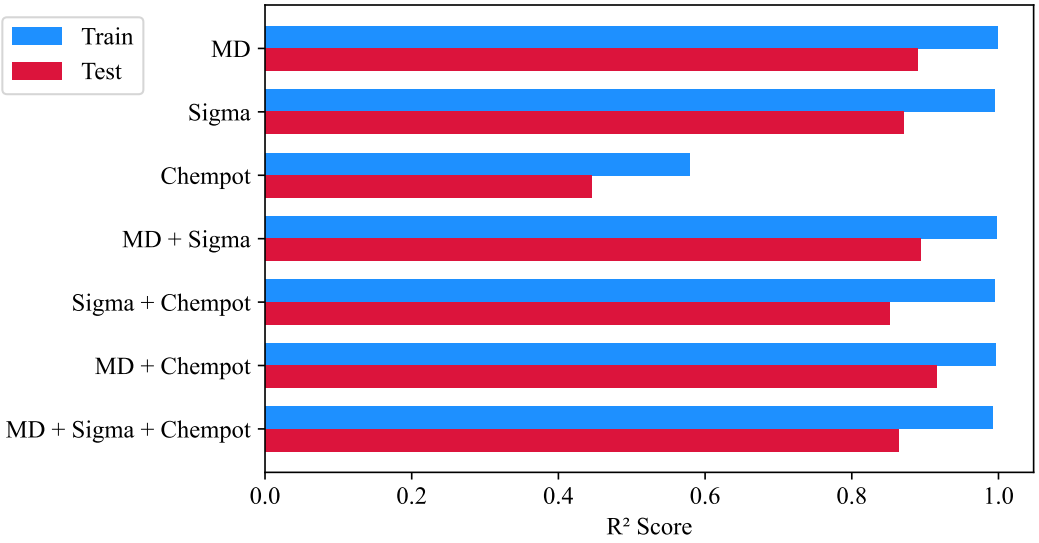

Fig. 5 Performance of pure IL viscosity models using different feature combinations (temperature is included in all cases).

B. Binary Mixture Viscosity Results

Many mixtures share similar structural motifs, and several composition combinations appear only once, which reduces uniqueness. As a result, model performance is highly sensitive to how the train/test split is constructed, and different test sets can lead to noticeably different R^2 scores. Figure 7 compares the performance of five different molecular descriptor mixing rules under two conditions: using all mixtures and using only mixtures at 50 mol%. Across both splitting strategies, the "square molar contribution" method emerged as the most stable and consistently accurate descriptor construction approach. In both cases, "square molar contribution" delivered strong test performance while maintaining a relatively small gap between training and test R^2 values. Because this descriptor strategy performed robustly in both the full composition and fixed composition scenarios, it was selected as the baseline MD representation for subsequent feature combination studies.

σ-profile integrals and chemical potential descriptors were incorporated to evaluate their contribution to mixture viscosity prediction. Figure 8 shows the results for each feature set under the two dataset splitting strategies. The overall trends reveal that σ-profile features alone provide surprisingly strong predictive capability, especially when the all mixture compositions data were used. In contrast, chemical-potential features alone show poor performance in the 50% mole-fraction case, even producing negative test R^2, but this behavior improves significantly when more data points are included. This again demonstrates that mixture modeling is highly sensitive to both the splitting strategy and the size of the training set. When combined with MDs, both sigma and chemical potential descriptors contribute positively, and hybrid feature sets such as "MD + Sigma + Chempot" or "Sigma + Chempot" achieve some of the most balanced performance across both splitting approaches.

Model behavior and feature importance patterns are explored further in Figs. 9 and 10. At 50 mol%, the sigma-only model achieves remarkably high accuracy ($R^2 = 0.989$), with temperature and a subset of sigma regions particularly σ_4,

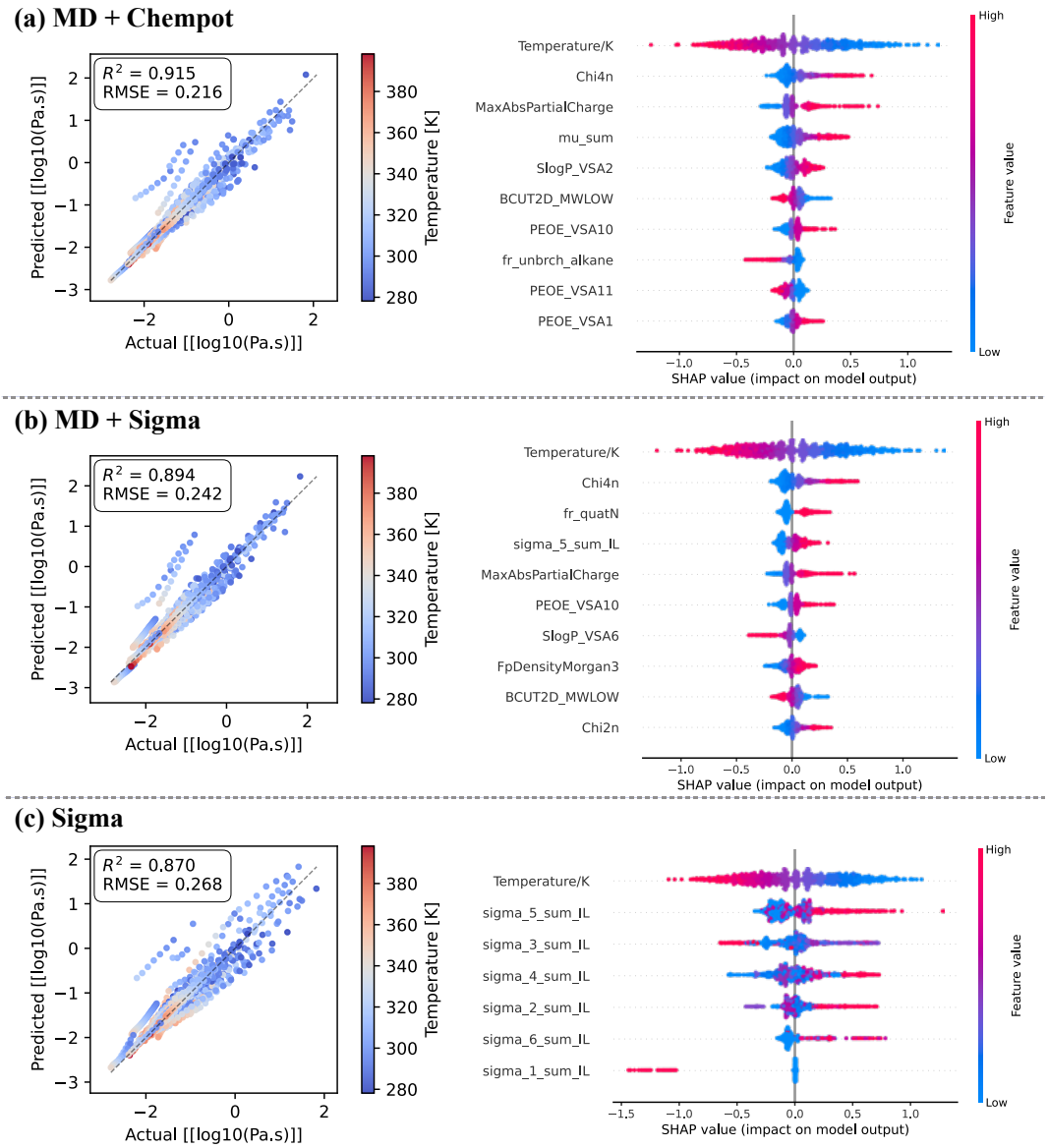

Fig. 6 Model performance and top 10 important features for pure IL viscosity predictions. (a) Molecular descriptor and chemical potential features. (b) Molecular descriptor and σ-profile features. (c) Only σ-profile features.

σ_2, and σ_5 driving the predictions. The "square molar contribution" MD model also performs well, with descriptors related to polarity, volume, and electronic state emerging as key contributors. While these performances are exceptionally high, it should be interpreted cautiously due to the limited data.

In the all-mixtures scenario, the best performing model combines chemical potential descriptors with "square molar contribution" MD features. Here, the global chemical potential measure (μ_{sum}) consistently appears among the top-ranked descriptors, reflecting its importance in capturing mixture specific energetic interactions. Adding sigma integrals on top of these features yields a small but meaningful improvement in generalization, particularly in distinguishing mixtures that differ only subtly in molecular structure or composition. The improved ML performance upon adding σ-profile and chemical-potential descriptors is consistent with recent findings as well, where σ-profiles serve as highly informative, physics-based molecular representations that capture polarity, charge distribution, and non-covalent interaction tendencies [41]. These properties strongly influence viscosity, particularly in mixtures where

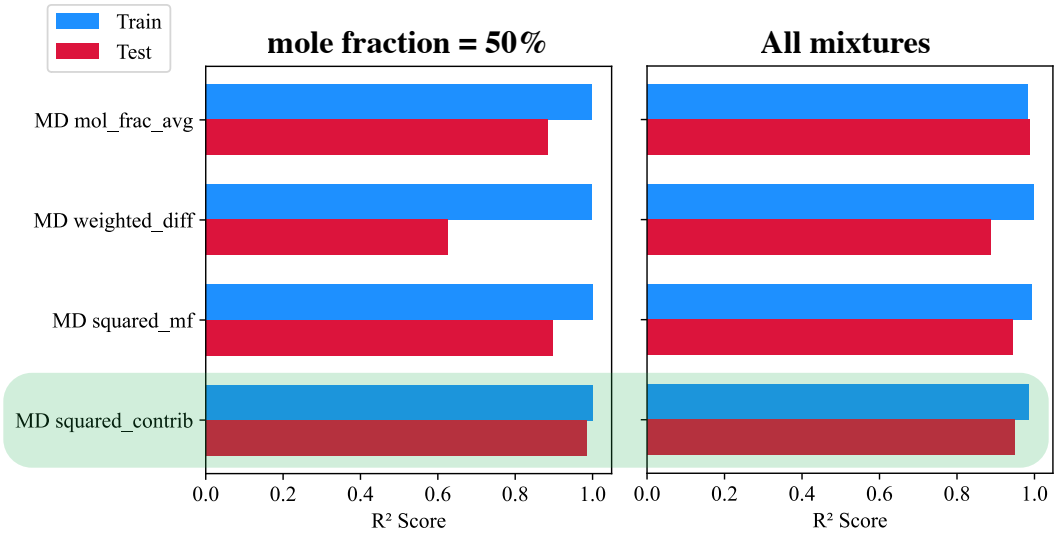

Fig. 7 Performance of binary mixture viscosity models using different molecular descriptor mixing rules under (left) 50 mol% fraction (right) all mixture data (temperature is included in all cases).

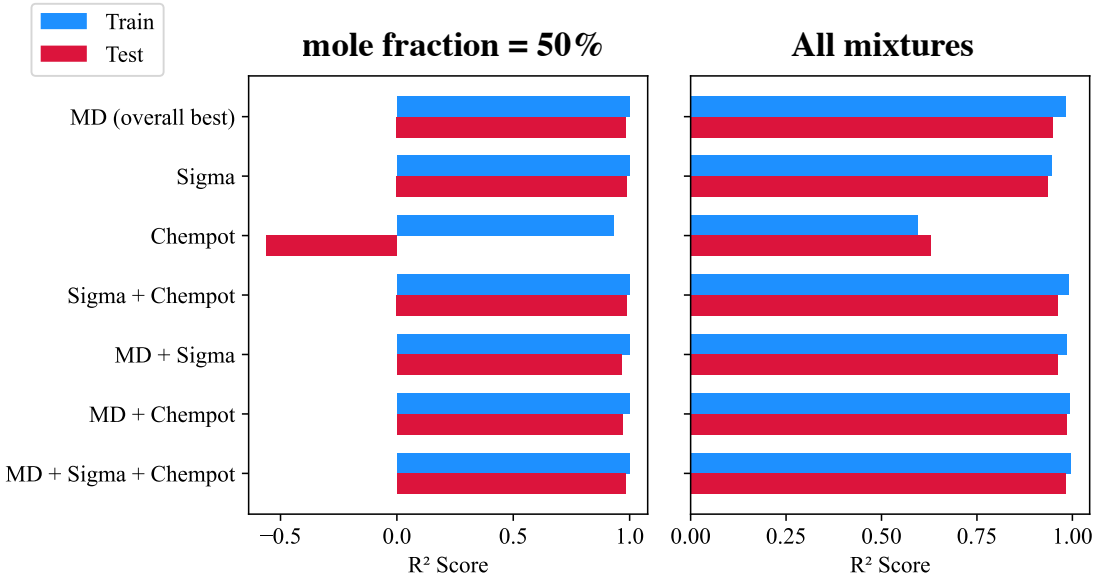

Fig. 8 Performance of binary mixture viscosity models using the best molecular descriptor mixing rule combined with sigma and chemical-potential features under (left) 50 mol% fraction (right) all mixture data (temperature is included in all cases).

composition-dependent interactions lead to nonlinear behavior. σ-profiles have also been shown to perform well even in small datasets, providing a compact and generalizable feature set. The chemical potential descriptors further incorporate local energetic interactions, enabling the model to better represent ion–ion interactions beyond what structural descriptors alone can encode.

Overall, the SHAP analyses reveal a consistent pattern: temperature is the strongest predictor in all models, followed by descriptors capturing molecular size, charge distribution, electronic environment, and surface polarity. These results reinforce the conclusion that, although binary mixtures are substantially more challenging to model than pure ILs, physics-based descriptors especially sigma integrals and chemical potentials provide complementary information that improves both predictive performance and interpretability.

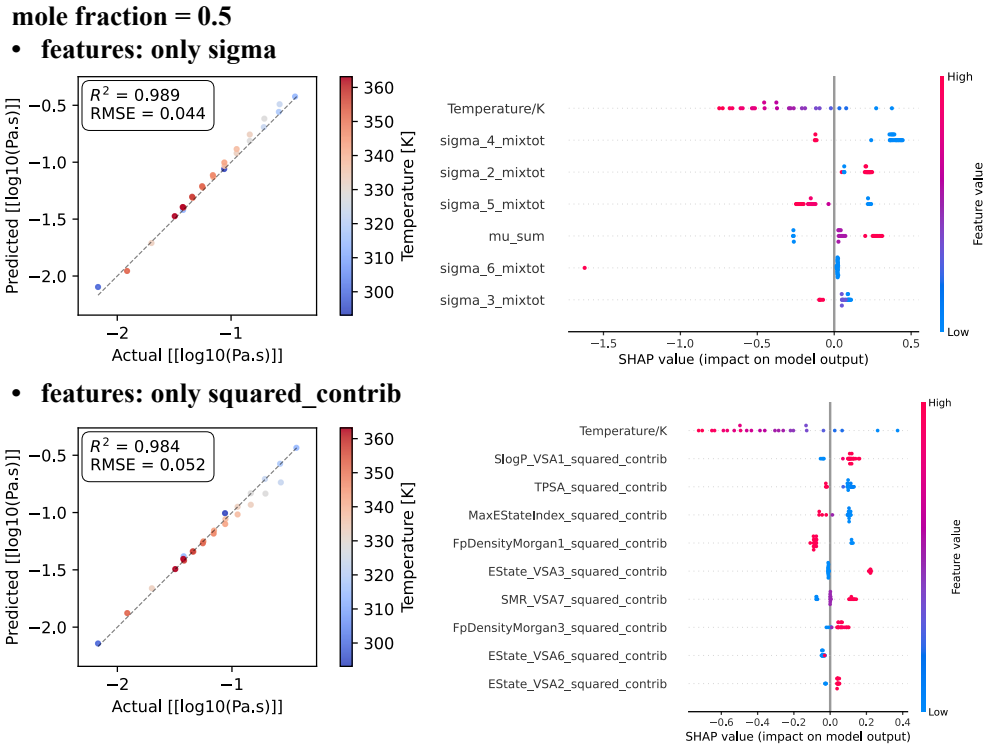

Fig. 9 Model performance and top 10 most important features for binary mixture viscosity predictions at 50% mole fraction for two of the best performing models.

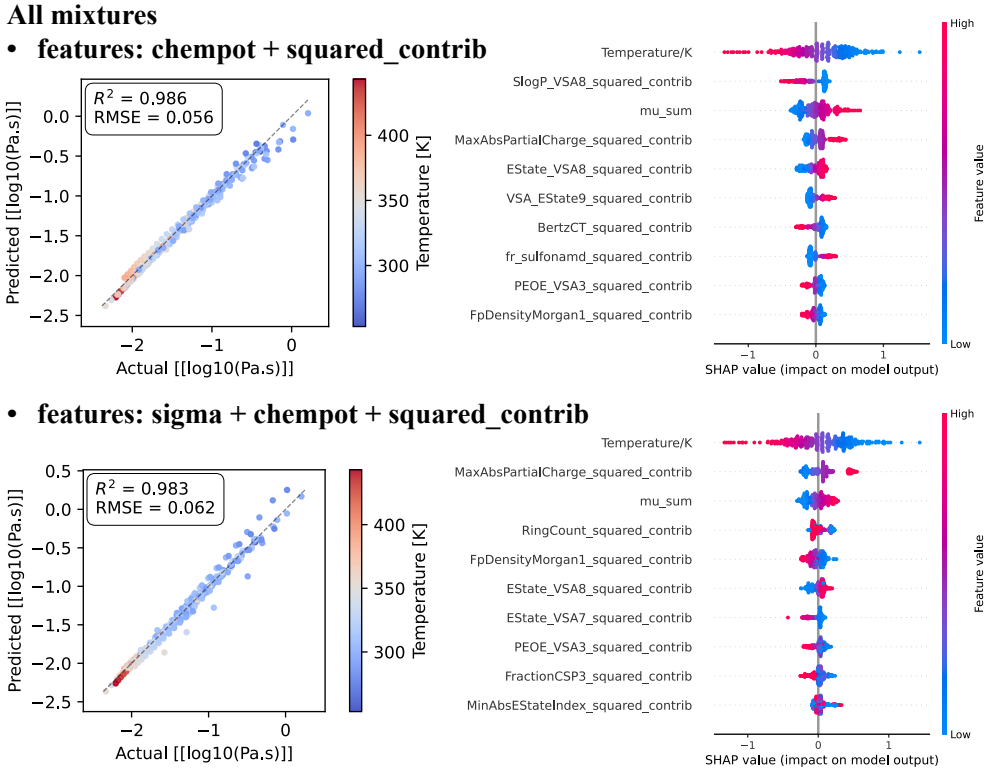

Fig. 10 Model performance and top 10 most important features for binary mixture viscosity predictions using all data, shown for two top-performing models.

IV. Conclusion

This study advances machine-learning approaches for predicting ionic liquid (IL) properties by incorporating physics-based descriptors and extending these methods to binary IL mixtures. In addition to conventional molecular descriptors, surface charge density features derived from σ-profiles and thermodynamic descriptors based on chemical potentials were introduced to better represent the intermolecular interactions that govern macroscopic transport behavior. The framework was evaluated for both pure ILs and binary mixtures to assess its broader applicability to systems with increasing compositional complexity.

For pure ILs, deep neural network models demonstrated strong predictive capability across all feature combinations, with the inclusion of σ-profile and chemical potential descriptors providing meaningful improvements in several cases. Feature importance analysis showed that σ-profile regions and chemical potential terms capture interaction physics that complement molecular descriptors, confirming that these additional descriptors contain information relevant to viscosity behavior.

Binary mixture modeling was more challenging due to limited data availability and low mixture uniqueness, which made performance highly sensitive to dataset splitting strategies. Among the molecular descriptor mixing rules, the square molar contribution formulation produced the most stable and consistent results and was therefore selected as the baseline representation. When physics-based features were added, σ-profile descriptors provided substantial predictive power, especially for fixed composition datasets, whereas chemical potential descriptors improved performance only when the mixture space was restricted. Hybrid feature sets combining molecular, σ-profile, and chemical potential descriptors yielded the most balanced and robust predictions across the different mixture scenarios. SHAP analysis highlighted the contributions of both structural and energetics-based descriptors, confirming their importance in capturing composition-dependent viscosity trends.

Overall, this work demonstrates that physics-based IL descriptors can complement molecular descriptor feature sets and noticeably enhance viscosity prediction for both pure ILs and binary mixtures. These results indicate that mixtures, when represented with appropriate descriptors, can achieve predictive accuracy comparable to pure ILs despite smaller dataset sizes. The framework developed here provides a foundation for large-scale mixture screening in future studies, enabling the identification of binary IL systems that offer improved viscosity behavior and broader tunability for thermal management applications. Future work will focus on expanding mixture datasets, refining energetic descriptor calculations, and extending the framework to additional thermophysical properties beyond viscosity to enable a more comprehensive, multi-property design of IL-based heat-transfer fluids. Integrating these models into iterative screening–synthesis–validation workflows will further accelerate the development of next-generation high-performance IL working fluids.

Acknowledgments

This work was supported by an Early Career Faculty award from NASA's Space Technology Research Grants Program (Grant No. 80NSSC23K1501). The authors would like to thank Tom Leimkuehler (NASA JSC) and Christopher Henry (NASA MSFC) for their valuable discussions and insightful feedback.

References

[1] Birur, G. C., Bhandari, P., Bame, D., Karlmann, P., Mastropietro, A. J., Liu, Y., Miller, J., Pauken, M., and Lyra, J., "From Concept to Flight: An Active Fluid Loop Based Thermal Control System for Mars Science Laboratory Rover," *42nd International Conference on Environmental Systems*, 2012. https://doi.org/10.2514/6.2012-3514.

[2] Ungar, E. K., and Erickson, L. R., "Assessment of the Use of Nanofluids in Spacecraft Active Thermal Control Systems," *AIAA SPACE 2011 Conference & Exposition*, AIAA 2011-7328, 2011. https://doi.org/10.2514/6.2011-7328.

[3] van Gerner, H., Van Benthem, R., van Es, J., Schwaller, D., and Lapensée, S., "Fluid Selection for Space Thermal Control Systems," *44th International Conference on Environmental Systems*, Tucson, 2014.

[4] Westheimer, D. T., and Tuan, G. C., "Active Thermal Control System Considerations for the Next Generation of Human Rated Space Vehicles," *43rd AIAA Aerospace Sciences Meeting and Exhibit - Meeting Papers*, 2005, pp. 1803–1807. https://doi.org/10.2514/6.2005-342.

[5] Gilmore, D., *Spacecraft Thermal Control Handbook, Volume I: Fundamental Technologies*, American Institute of Aeronautics and Astronautics, Inc., Washington, DC, 2002. https://doi.org/10.2514/4.989117.

[6] Evich, M. G., Davis, M. J., McCord, J. P., Acrey, B., Awkerman, J. A., Knappe, D. R., Lindstrom, A. B., Speth, T. F., Tebes-Stevens, C., Strynar, M. J., Wang, Z., Weber, E. J., Henderson, W. M., and Washington, J. W., "Per- and polyfluoroalkyl substances in the environment," *Science*, Vol. 375, No. 6580, 2022. https://doi.org/10.1126/science.abg9065.

[7] Harrad, S., Abdallah, M. A. E., Drage, D., and Meyer, M., "Persistent Organic Contaminants in Dust from the International Space Station," *Environmental Science and Technology Letters*, Vol. 10, No. 9, 2023, pp. 768–772. https://doi.org/10.1021/acs.estlett.3c00448.

[8] Ng, C., Cousins, I. T., DeWitt, J. C., Glüge, J., Goldenman, G., Herzke, D., Lohmann, R., Miller, M., Patton, S., Scheringer, M., Trier, X., and Wang, Z., "Addressing Urgent Questions for PFAS in the 21st Century," , 10 2021. https://doi.org/10.1021/acs.est.1c03386.

[9] Chaubey, A. K., Pratap, T., and Mohan, D., "Growing Concern about Per- and Polyfluoroalkyl Substance (PFAS) Contamination: An Emerging Environmental Challenge and Its Management," *ACS Sustainable Resource Management*, 2025. https://doi.org/10.1021/acssusresmgt.5c00376.

[10] Ateia, M., and Scheringer, M., "From "forever chemicals" to fluorine-free alternatives," *Science*, Vol. 385, No. 6706, 2024, pp. 256–258. https://doi.org/10.1126/science.ado5019.

[11] Paris, A. D., Bhandari, P., and Birur, G. C., "High Temperature Mechanically Pumped Fluid Loop for Space Applications –Working Fluid Selection," 2004. https://doi.org/10.4271/2004-01-2415.

[12] Acar, E., and Sobhani, S., "Predicting Thermophysical Properties of Ionic Liquids Using Deep Neural Networks and Random Forests," *AIAA Science and Technology Forum and Exposition, AIAA SciTech Forum 2025*, American Institute of Aeronautics and Astronautics Inc, AIAA, 2025. https://doi.org/10.2514/6.2025-1223.

[13] Minea, A. A., "Overview of Ionic Liquids as Candidates for New Heat Transfer Fluids," *International Journal of Thermophysics*, Vol. 41, No. 11, 2020. https://doi.org/10.1007/s10765-020-02727-3.

[14] Kazakov, A., Magee, J., Chirico, R., Diky, V., Kroenlein, K., Muzny, C., and Frenkel, M., "Ionic Liquids Database - ILThermo (v2.0)," , 11 2013. URL http://trcsrv1.boulder.nist.gov/ilthermo/ilthermo.html(AccessedAugust18,2024).

[15] Annat, G., Forsyth, M., and MacFarlane, D. R., "Ionic liquid mixtures-variations in physical properties and their origins in molecular structure," *Journal of Physical Chemistry B*, Vol. 116, No. 28, 2012, pp. 8251–8258. https://doi.org/10.1021/jp3012602.

[16] Chatel, G., Pereira, J. F., Debbeti, V., Wang, H., and Rogers, R. D., "Mixing ionic liquids-"simple mixtures" or "double salts"?" , 2014. https://doi.org/10.1039/c3gc41389f.

[17] Niedermeyer, H., Hallett, J. P., Villar-Garcia, I. J., Hunt, P. A., and Welton, T., "Mixtures of ionic liquids," *Chemical Society Reviews*, Vol. 41, No. 23, 2012, pp. 7780–7802. https://doi.org/10.1039/c2cs35177c.

[18] Gaudin, T., Rotureau, P., and Fayet, G., "Mixture Descriptors toward the Development of Quantitative Structure-Property Relationship Models for the Flash Points of Organic Mixtures," *Industrial and Engineering Chemistry Research*, Vol. 54, No. 25, 2015, pp. 6596–6604. https://doi.org/10.1021/acs.iecr.5b01457.

[19] Fu, Y., Liu, X., Gao, J., Lei, Y., Chen, Y., and Zhang, X., "Machine learning models for the density and heat capacity of ionic liquid–water binary mixtures," *Chinese Journal of Chemical Engineering*, Vol. 73, 2024, pp. 244–255. https://doi.org/10.1016/j.cjche.2024.04.019.

[20] Mohan, M., Jetti, K. D., Guggilam, S., Smith, M. D., Kidder, M. K., and Smith, J. C., "High-Throughput Screening and Accurate Prediction of Ionic Liquid Viscosities Using Interpretable Machine Learning," *ACS Sustainable Chemistry and Engineering*, Vol. 12, No. 18, 2024, pp. 7040–7054. https://doi.org/10.1021/acssuschemeng.4c00631.

[21] Keller, A. N., Kelkar, P., Baldea, M., Stadtherr, M. A., and Brennecke, J. F., "Thermophysical property prediction of anion-functionalized ionic liquids for CO2 capture," *Journal of Molecular Liquids*, Vol. 393, 2024. https://doi.org/10.1016/j.molliq.2023.123634.

[22] Chen, Y., Ma, S., Lei, Y., Liang, X., Liu, X., Kontogeorgis, G. M., and Gani, R., "Ionic liquid binary mixtures: Machine learning-assisted modeling, solvent tailoring, process design, and optimization," *AIChE Journal*, Vol. 70, No. 5, 2024. https://doi.org/10.1002/aic.18392.

[23] Huwaimel, B., Alanazi, J., Alanazi, M., Alharby, T. N., and Alshammari, F., "Computational models based on machine learning and validation for predicting ionic liquids viscosity in mixtures," *Scientific Reports*, Vol. 14, No. 1, 2024. https://doi.org/10.1038/s41598-024-82989-1.

[24] Gao, N., Yang, Y., Wang, Z., Guo, X., Jiang, S., Li, J., Hu, Y., Liu, Z., and Xu, C., "Viscosity of Ionic Liquids: Theories and Models," , 1 2024. https://doi.org/10.1021/acs.chemrev.3c00339.

[25] Dong, Q., Muzny, C., Kazakov, A., Diky, V., Magee, J., Widegren, J., Chirico, R., Marsh, K., and Frenkel, M., "ILThermo: A Free-Access Web Database for Thermodynamic Properties of Ionic Liquids," *Journal of Chemical & Engineering Data*, Vol. 52, No. 4, 2007, pp. 1151–1159. https://doi.org/10.1021/je700171f.

[26] Lowe, D. M., Corbett, P. T., Murray-Rust, P., and Glen, R. C., "Chemical Name to Structure: OPSIN, an Open Source Solution," *Journal of Chemical Information and Modeling*, Vol. 51, No. 3, 2011, pp. 739–753. https://doi.org/10.1021/ci100384d.

[27] Landrum, G., Tosco, P., Kelley, B., Ric, Cosgrove, D., sriniker, Vianello, R., gedeck, NadineSchneider, Jones, G., Kawashima, E., N, D., Dalke, A., Cole, B., Swain, M., Turk, S., Savelev, A., Vaucher, A., Wójcikowski, M., Take, I., Scalfani, V. F., Probst, D., Ujihara, K., godin, g., Pahl, A., Walker, R., Lehtivarjo, J., Berenger, F., strets123, and jasondbiggs, "rdkit/rdkit: Release_2023.09.5," Zenodo, 2024. https://doi.org/10.5281/zenodo.10633624.

[28] Acar, Z., Nguyen, P., Cui, X., and Lau, K. C., "Room Temperature Ionic Liquids Viscosity Prediction from Deep-Learning Models," *Energy Materials*, 2023. https://doi.org/10.20517/energymater.2023.38.

[29] Koutsoukos, S., Philippi, F., Malaret, F., and Welton, T., "A Review on Machine Learning Algorithms for the Ionic Liquid Chemical Space," *Chemical Science*, Vol. 12, No. 20, 2021, pp. 6820–6843. https://doi.org/10.1039/d1sc01000j.

[30] Datta, R., Ramprasad, R., and Venkatram, S., "Conductivity Prediction Model for Ionic Liquids Using Machine Learning," *Journal of Chemical Physics*, Vol. 156, No. 21, 2022. https://doi.org/10.1063/5.0089568.

[31] Bendimerad, R., and Petro, E., "Discovery of ionic liquid propellants for electrospray thrusters using molecular descriptors and machine learning," *Journal of Electric Propulsion*, Vol. 4, No. 1, 2025. https://doi.org/10.1007/s44205-025-00143-z.

[32] Baskin, I., Epshtein, A., and Ein-Eli, Y., "Benchmarking machine learning methods for modeling physical properties of ionic liquids," *Journal of Molecular Liquids*, Vol. 351, 2022. https://doi.org/10.1016/j.molliq.2022.118616.

[33] Shao, Y., Wang, Z., Wang, L., Kuai, Y., Gao, R., and Zhang, C., "Machine learning-based structure—property modeling for ionic liquids design and screening: A state-of-the-art review," , 2025. https://doi.org/10.1007/s11708-025-1011-7.

[34] Pedregosa, F., Varoquaux, G., Gramfort, A., Michel, V., Thirion, B., Grisel, O., Blondel, M., Prettenhofer, P., Weiss, R., Dubourg, V., Vanderplas, J., Passos, A., Cournapeau, D., Brucher, M., Perrot, M., and Duchesnay, E., "Scikit-learn: Machine Learning in Python," *Journal of Machine Learning Research*, Vol. 12, 2011, pp. 2825–2830.

[35] Tibshirani, R., "Regression Shrinkage and Selection via the Lasso," *Journal of the Royal Statistical Society. Series B (Methodological)*, Vol. 58, No. 1, 1996, pp. 267–288. URL http://www.jstor.org.proxy.library.cornell.edu/stable/2346178.

[36] Pye, C. C., Ziegler, T., Lenthe, E. V., and Louwen, J. N., "An implementation of the conductor-like screening model of solvation within the amsterdam density functional package - Part II. COSMO for real solvents," *Canadian Journal of Chemistry*, Vol. 87, No. 7, 2009, pp. 790–797. https://doi.org/10.1139/V09-008.

[37] Louwen, J., Pye, C., van Lenthe, E., Austin, N., McGarrity, E., Xiong, R., Sandler, S., and Burnett, R., "AMS 2025.1 COSMO-RS, SCM, Theoretical Chemistry, Vrije Universiteit, Amsterdam, The Netherlands,," , 2025.

[38] Klamt, A., Eckert, F., and Arlt, W., "COSMO-RS: An alternative to simulation for calculating thermodynamic properties of liquid mixtures," *Annual Review of Chemical and Biomolecular Engineering*, Vol. 1, 2010, pp. 101–122. https://doi.org/10.1146/annurev-chembioeng-073009-100903.

[39] Kingma, D. P., and Ba, J., "Adam: A Method for Stochastic Optimization," 2014. URL http://arxiv.org/abs/1412.6980.

[40] Lundberg, S., and Lee, S.-I., "A Unified Approach to Interpreting Model Predictions," 2017. URL http://arxiv.org/abs/1705.07874.

[41] Abranches, D. O., Zhang, Y., Maginn, E. J., and Colón, Y. J., "Sigma profiles in deep learning: towards a universal molecular descriptor," *Chemical Communications*, 2022. https://doi.org/10.1039/d2cc01549h.